

# A Plate Bending Kirchhoff Element Based on Assumed Strain Functions

F. Boussem<sup>1,\*</sup>, L. Belouar<sup>2</sup>

<sup>1</sup>*Biskra University, BP145 Biskra 07000, Algeria*

<sup>2</sup>*NMISSI Laboratory, Biskra University, BP145 Biskra 07000, Algeria*

Received 5 August 2020; accepted 5 October 2020

## ABSTRACT

To investigate static and free vibration for thin plate bending structures, a four-node quadrilateral finite element is proposed in this research paper. This element has been formulated by using both the assumptions of thin plates theory (Kirchhoff plate theory) and strain approach. The suggested element which possesses only three degrees of freedom (one transverse displacement and two normal rotations) at each of four corner nodes is based on assumed higher-order functions for the various components of strain field that satisfies the compatibility equation. The displacement functions of the developed element are obtained by integrating the assumed strains functions and satisfy the exact representation of the rigid body modes. Several numerical tests in both static and free vibration analysis are presented to assess the performance of the new element. The obtained results show high solution accuracy, especially for coarse meshes, of the developed element compared with analytical and other numerical solutions available in the literature. © 2020 IAU, Arak Branch. All rights reserved.

**Keywords:** Strain approach; Plate bending; Kirchhoff plate theory; Higher-order strain field; Free vibration.

## 1 INTRODUCTION

PLATE are defined as plane structural in which the thickness is very small compared to other planar dimensions [1]. The analyses of plates are classified into two categories thick plate and thin plate analysis. The Reissner-Mindlin plate theory has been generally applied in the developing of thick plates which take into account transverse shear deformation through the plate thickness. Thin plates analysis which ignored the transverse shear deformation is based on Kirchhoff plate theory. First previous plate elements are based on the classical Kirchhoff thin plate theory which C1 continuity between adjacent elements is required, the construction procedures of Kirchhoff plate elements are difficult and more complicated [2]. Several researchers have developed reliable and efficient plate bending elements that are being used to analyze thin plate problems. A successful non-conforming rectangular ACM plate element was developed by Melosh [3]. This element had twelve degrees of freedom (DOFs) and used a complete third order polynomial expansion in  $x$  and  $y$ . Many other successful finite elements were

\*Corresponding author. Tel.: +213 671181174.  
E-mail address: boussem-faycal@univ-adrar.dz (F. Boussem)

formulated for analysis of thin-plate bending. For example, the discrete Kirchhoff theory has been efficiently used by several researchers to develop some thin plate elements [4-5], and the hybrid formulation which has an immense capacity in constructing useful finite elements for the analysis of the plate bending structures. Based on this methodology, the most recent method called Hybrid-Trefftz (HT) was developed for the analysis of thin bending plates. The advantages of this technique have attracted many researchers to develop several plate bending elements [6-7]. Another model has been adopted, referred to as the strain-based or the strain approach. In this approach, the displacements field of finite element is based on an assumed function for the various components of strain field that satisfies the compatibility equations. The advantages of strain approach are the satisfaction of the two main convergence criteria directly related to the strains (constant strains and rigid body movement) and the possibility of enriching the displacement field by high order terms without the need of inclusion of intermediate nodes or of additional non-essential degrees of freedom [8]. The strain approach is very effective in solving problems such as parasitic errors, distortion mesh, and various locking phenomena [9]. The first finite elements based on strain approach were curved elements. This formulation was used for the arcs analysis by Ashwell, Sabir, and Roberts [10] and for the analysis of cylindrical shells by Ashwell and Sabir [11]. This approach was later applied to analyzing thick plates. Belouar and Guenfoud [12] developed the first plate bending element based on the strain-based approach and the Reissner-Mindlin theory. This element suffers from some shear locking as the plate becomes progressively thinner. The success of the strain approach has been confirmed by several 3D plate elements [13-17] and Reissner-Mindlin plate elements [18-20]. This has motivated the authors to propose the first quadrilateral finite element based on Kirchhoff plate theory and higher-order strain field. The proposed finite element is simple in the formulation and effective for both static and free vibration analysis.

The objective of this paper is to evaluate the performance of strain approach to develop a four-node quadrilateral element based on Kirchhoff plate theory for plates bending problems. This new element called KSBQP (Kirchhoff Strain Based Quadrilateral Plate) was developed to investigate the effect of higher-order strain states on the accuracy of plates test results. This element which contains three degrees of freedom per node is tested for static and free vibration analysis of plates bending structures. The obtained results are compared with those of other finite elements and analytical solutions given in the literature.

## 2 FORMULATION OF THE QUADRILATERAL ELEMENT KSBQP

### 2.1 Displacements field for the strain-based plate element

Fig. 1 shows a quadrilateral element (KSBQP) having three degrees of freedom, the displacement component along the thickness ( $W$ ) and two rotations  $\beta_x = \theta_y$  and  $\beta_y = -\theta_x$  at each of the four corner nodes. The strain displacement equations for a thin plate element are given by:

$$\begin{aligned}\varepsilon_x &= \frac{\partial u}{\partial x} = z \frac{\partial \beta_x}{\partial x} = -z \frac{\partial^2 W}{\partial x^2} \\ \varepsilon_y &= \frac{\partial v}{\partial y} = z \frac{\partial \beta_y}{\partial y} = z \frac{\partial^2 W}{\partial y^2} \\ \gamma_{xy} &= \left( \frac{\partial u}{\partial y} + \frac{\partial v}{\partial x} \right) = z \left( \frac{\partial \beta_x}{\partial y} + \frac{\partial \beta_y}{\partial x} \right) = -2z \frac{\partial^2 W}{\partial x \partial y} \\ \gamma_{xz} &= \gamma_{zx} = 0\end{aligned}\tag{1}$$

The bending curvatures are given by equation:

$$\begin{aligned}\kappa_x &= \frac{\partial \beta_x}{\partial x} = -\frac{\partial^2 W}{\partial x^2} \\ \kappa_y &= \frac{\partial \beta_y}{\partial y} = -\frac{\partial^2 W}{\partial y^2} \\ \kappa_{xy} &= \left( \frac{\partial \beta_x}{\partial y} + \frac{\partial \beta_y}{\partial x} \right) = -2 \frac{\partial^2 W}{\partial x \partial y}\end{aligned}\tag{2}$$

where the above three bending curvatures given by Eq. (2) cannot be considered independent, for they are in terms of the displacements  $W$ ,  $\beta_x$  and  $\beta_y$ , and therefore, they must satisfy the compatibility equations given as:

$$\begin{aligned} \frac{\partial^2 \kappa_x}{\partial y^2} + \frac{\partial^2 \kappa_y}{\partial x^2} &= \frac{\partial^2 \kappa_{xy}}{\partial x \partial y} \\ \frac{\partial^2 \gamma_{xz}}{\partial x \partial y} - \frac{\partial^2 \gamma_{yz}}{\partial x^2} + \frac{\partial \kappa_{xy}}{\partial x} &= 2 \frac{\partial \kappa_x}{\partial y} \\ \frac{\partial^2 \gamma_{yz}}{\partial x \partial y} - \frac{\partial^2 \gamma_{xz}}{\partial y^2} + \frac{\partial \kappa_{xy}}{\partial y} &= 2 \frac{\partial \kappa_y}{\partial x} \end{aligned} \tag{3}$$

First the displacements field corresponding to the three rigid-body modes (MCR) is obtained by equating the three bending curvatures given in Eq. (2) to zero and integrating the resulting differential equations to obtain:

$$W = \alpha_1 - \alpha_2 x - \alpha_3 y \quad \beta_x = \alpha_2 \quad \beta_y = \alpha_3 \tag{4}$$

with  $\alpha_2$  and  $\alpha_3$  parameters representing rotations  $\theta_x$  and  $\theta_y$  of the rigid body about respective axis  $y$  and  $x$  and  $\alpha_1$  representing translation of the rigid body along the normal axis  $z$ .

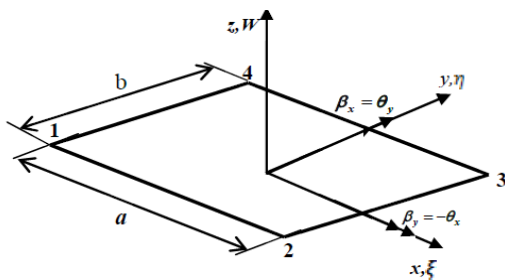


**Fig.1**  
Geometry of the quadrilateral element KSBQP.

The proposed element has three degrees of freedom ( $W$ ,  $\beta_x$  and  $\beta_y$ ) at each of four corner nodes. Therefore, the displacements field should contain twelve independent constants and having used three ( $\alpha_1, \alpha_2, \alpha_3$ ) for the representation of the rigid body modes, the remaining nine constants ( $\alpha_4, \alpha_5, \dots, \alpha_{12}$ ) are used to express the displacements corresponding to straining of the element. These are apportioned among the strain as follows:

$$\begin{aligned} \kappa_x &= \alpha_4 + x \alpha_5 + y \alpha_6 + xy \alpha_7 + x^2 \alpha_9 \\ \kappa_y &= \alpha_8 + x \alpha_9 + y \alpha_{10} + xy \alpha_{11} + y^2 \alpha_6 \\ \kappa_{xy} &= \alpha_{12} + (x^2 \alpha_7 + y^2 \alpha_{11} + 2x \alpha_6 + 2y \alpha_9) \end{aligned} \tag{5}$$

The un-bracketed terms in Eq. (5) are assumed.  $\alpha_4, \alpha_8$  and  $\alpha_{12}$  are the terms corresponding to constant strain states to ensure convergence as the finite element grid is refined. The higher order bracketed terms are then added to satisfy the compatibility Eq. (3). The assumed strains given by Eq. (5) are substituted into Eq.(2) and the resulting equations are integrated to obtain the following field:

$$\begin{aligned} W &= -\frac{x^2}{2} \alpha_4 - \frac{x^3}{6} \alpha_5 - \left( \frac{x^2 y}{2} + \frac{y^4}{12} \right) \alpha_6 - \frac{x^3 y}{6} \alpha_7 - \frac{y^2}{2} \alpha_8 - \left( \frac{y^2 x}{2} + \frac{x^4}{12} \right) \alpha_9 - \frac{y^3}{6} \alpha_{10} - \frac{y^3 x}{6} \alpha_{11} - \frac{xy}{2} \alpha_{12} \\ \beta_x &= x \alpha_4 + \frac{x^2}{2} \alpha_5 + xy \alpha_6 + \frac{x^2 y}{2} \alpha_7 + \left( \frac{y^2}{2} + \frac{x^3}{3} \right) \alpha_9 + \frac{y^3}{6} \alpha_{11} + \frac{y}{2} \alpha_{12} \\ \beta_y &= \left( \frac{x^2}{2} + \frac{y^3}{3} \right) \alpha_6 + \frac{x^3}{6} \alpha_7 + y \alpha_8 + xy \alpha_9 + \frac{y^2}{2} \alpha_{10} + \frac{xy^2}{2} \alpha_{11} + \frac{x}{2} \alpha_{12} \end{aligned} \tag{6}$$

The complete displacement shape functions are the sum of corresponding expressions from Eqs.(4) and (6):

$$\begin{aligned}
 W &= \alpha_1 - \alpha_2 x - \alpha_3 y - \frac{x^2}{2} \alpha_4 - \frac{x^3}{6} \alpha_5 - \left( \frac{x^2 y}{2} + \frac{y^4}{12} \right) \alpha_6 - \frac{x^3 y}{6} \alpha_7 - \frac{y^2}{2} \alpha_8 - \left( \frac{y^2 x}{2} + \frac{x^4}{12} \right) \alpha_9 - \frac{y^3}{6} \alpha_{10} - \frac{y^3 x}{6} \alpha_{11} - \frac{xy}{2} \alpha_{12} \\
 \beta_x &= \alpha_2 + x \alpha_4 + \frac{x^2}{2} \alpha_5 + xy \alpha_6 + \frac{x^2 y}{2} \alpha_7 + \left( \frac{y^2}{2} + \frac{x^3}{3} \right) \alpha_9 + \frac{y^3}{6} \alpha_{11} + \frac{y}{2} \alpha_{12} \\
 \beta_y &= \alpha_3 + \left( \frac{x^2}{2} + \frac{y^3}{3} \right) \alpha_6 + \frac{x^3}{6} \alpha_7 + y \alpha_8 + xy \alpha_9 + \frac{y^2}{2} \alpha_{10} + \frac{xy^2}{2} \alpha_{11} + \frac{x}{2} \alpha_{12}
 \end{aligned} \tag{7}$$

The displacement functions of Eq. (7) and the strain functions of Eq. (5) can be given in matrix form, respectively, as:

$$\{U\} = [P] \{\alpha\} \tag{8}$$

$$\{\varepsilon\} = [Q] \{\alpha\} \tag{9}$$

with  $\{\alpha\} = \{\alpha_1, \alpha_2, \dots, \alpha_{12}\}^T$

$$[P] = \begin{bmatrix} 1 & -x & -y & -\frac{x^2}{2} & -\frac{x^3}{6} & -\left(\frac{x^2 y}{2} + \frac{y^4}{12}\right) & -\frac{x^3 y}{6} & -\frac{y^2}{2} & -\left(\frac{y^2 x}{2} + \frac{x^4}{12}\right) & -\frac{y^3}{6} & -\frac{y^3 x}{6} & -\frac{xy}{2} \\ 0 & 1 & 0 & x & \frac{x^2}{2} & xy & \frac{x^2 y}{2} & 0 & \left(\frac{y^2}{2} + \frac{x^3}{3}\right) & 0 & \frac{y^3}{6} & \frac{y}{2} \\ 0 & 0 & 1 & 0 & 0 & \left(\frac{y^3}{3} + \frac{x^2}{2}\right) & \frac{x^3}{6} & y & xy & \frac{y^2}{2} & \frac{y^2 x}{2} & \frac{x}{2} \end{bmatrix} \tag{10}$$

$$[Q] = \begin{bmatrix} 0 & 0 & 0 & 1 & x & y & xy & 0 & x^2 & 0 & 0 & 0 \\ 0 & 0 & 0 & 0 & 0 & y^2 & 0 & 1 & x & y & xy & 0 \\ 0 & 0 & 0 & 0 & 0 & 2x & x^2 & 0 & 2y & 0 & y^2 & 1 \end{bmatrix} \tag{11}$$

The transformation matrix  $[C]$  which relates the vector of the element nodal displacements  $\{q_e\}$  to the vector of constants  $\{\alpha\}$  as:

$$\{q_e\} = [C] \{\alpha\} \tag{12}$$

with:

$$\{q_e\}^T = \{W_1, \beta_{x1}, \beta_{y1}, W_2, \beta_{x2}, \beta_{y2}, W_3, \beta_{x3}, \beta_{y3}, W_4, \beta_{x4}, \beta_{y4}\}$$

and the transformation matrix  $[C]$  ( $12 \times 12$ ) for the KSBQP element is as follows:

$$[C] = \begin{bmatrix} P_1(x_1, y_1) \\ P_2(x_2, y_2) \\ P_3(x_3, y_3) \\ P_4(x_4, y_4) \end{bmatrix} \tag{13}$$

where the matrix  $[P_i(x_i, y_i)]$  is calculated from Eq. (10) for each of the four element nodes coordinates  $(x_i, y_i)$ , ( $i= 1, 2, 3, 4$ ), to obtain:

$$[P_i(x_i, y_i)] = \begin{bmatrix} 1 & -x_i & -y_i & -\frac{x_i^2}{2} & -\frac{x_i^3}{6} & -\left(\frac{x_i^2 y_i + y_i^4}{2} + \frac{y_i^4}{12}\right) & -\frac{x_i^3 y_i}{6} & -\frac{y_i^2}{2} & -\left(\frac{y_i^2 x_i + x_i^4}{2} + \frac{x_i^4}{12}\right) & -\frac{y_i^3}{6} & -\frac{y_i^3 x_i}{6} & -\frac{x_i y_i}{2} \\ 0 & 1 & 0 & x_i & \frac{x_i^2}{2} & x_i y_i & \frac{x_i^2 y_i}{2} & 0 & \left(\frac{y_i^2 + x_i^3}{2} + \frac{x_i^3}{3}\right) & 0 & \frac{y_i^3}{6} & \frac{y_i}{2} \\ 0 & 0 & 1 & 0 & 0 & \left(\frac{y_i^3 + x_i^2}{3} + \frac{x_i^2}{2}\right) & \frac{x_i^3}{6} & y_i & x_i y_i & \frac{y_i^2}{2} & \frac{y_i^2 x_i}{2} & \frac{x_i}{2} \end{bmatrix} \quad (14)$$

The constant parameters vector  $\{a\}$  can be derived from Eq. (12) as follow:

$$\{a\} = [C]^{-1} \{q_e\} \quad (15)$$

By substituting Eq. (15) into Eqs. (8) and (9) we obtain:

$$\{U\} = [P][C]^{-1} \{q_e\} = [N] \{q_e\} \quad (16)$$

$$\{\varepsilon\} = [Q(x, y)][C]^{-1} \{q_e\} = [B] \{q_e\} \quad (17)$$

with:

$$[N] = [P][C]^{-1}; \quad [B] = [Q(x, y)][C]^{-1} \quad (18)$$

The stress-strain relationship is given by:

$$\{\sigma\} = [D] \{\varepsilon\} \quad (19)$$

where

$$\{\sigma\} = \{M_x, M_y, M_{xy}\}^T; \quad \{\varepsilon\} = \{\kappa_x, \kappa_y, \kappa_{xy}\}^T$$

and the elasticity matrix  $[D]$  is:

$$[D] = \begin{bmatrix} D_{11} & D_{12} & 0 \\ D_{21} & D_{22} & 0 \\ 0 & 0 & D_{33} \end{bmatrix} \quad (20)$$

where:

$$D_{11} = D_{22} = \frac{Eh^3}{(1-\nu^2)}; \quad D_{12} = D_{21} = \nu D_{11}; \quad D_{33} = D_{11} \frac{(1-\nu)}{2}$$

### 2.2 Element stiffness and mass matrices

For static and free vibration, the standard weak form can, respectively, be expressed as:

$$\int_{V_e} \delta \{\varepsilon\}^T [\sigma] dV = \int_{V_e} \delta \{U\}^T \{f_v\} dV \quad (21)$$

$$\int_{V_e} \delta \{\varepsilon\}^T [\sigma] dV + \int_{V_e} \delta \{U\}^T \{U\} dV = 0 \quad (22)$$

By substituting Eqs. (16), (17) and (19) into Eqs. (21) and (22), we obtain:

$$\delta \{q_e\}^T \left( \int_{V_e} [B]^T [D] [B] dV \right) \{q_e\} = \delta \{q_e\}^T \left( \int_{V_e} [N]^T \{f_v\} dV \right) \quad (23)$$

$$\delta \{q_e\}^T \left( \int_{V_e} [B]^T [D] [B] dV \right) \{q_e\} + \delta \{q_e\}^T \left( \int_{V_e} \rho [N]^T [N] dV \right) \{q_e\} = 0 \quad (24)$$

where the element stiffness  $[K^e]$  and mass  $[M^e]$  matrices are, respectively, given as:

$$[K^e] = \int_{V_e} [B]^T [D] [B] dV = [C]^T \underbrace{\left( \int_{V_e} [Q]^T [D] [Q] \det(J) d\xi d\eta \right)}_{[K_0]} [C]^{-1} \quad (25)$$

$$[M^e] = \rho h \int_{V_e} [N]^T [N] dV = [C]^T \underbrace{\left( \int_{V_e} [P]^T [P] \det(J) d\xi d\eta \right)}_{[M_0]} [C]^{-1} \quad (26)$$

and the element nodal body forces vector is:

$$\{F_b\} = \int_{V_e} [N]^T \{f_v\} dV = [C]^T \int_{V_e} [P]^T \{f_v\} dV \quad (27)$$

The matrices  $[K_0]$  and  $[M_0]$  given in Eqs. (25) and (26) are numerically computed with exact Gauss integration. The element stiffness and mass matrices ( $[K^e]$  and  $[M^e]$ ) can then be obtained. These are assembled to obtain the structural stiffness and mass matrices ( $[K]$  and  $[M]$ ).

For static analysis, we use:

$$[K] \{q\} = \{F\} \quad (28)$$

For free vibration, we use:

$$([K] - \omega^2 [M]) \{q\} = 0 \quad (29)$$

where  $\{q\}$  is the structural global displacements vector.

### 3 NUMERICAL VALIDATION

#### 3.1 Static analysis

##### 3.1.1 Square plate analysis

A square plate of length  $L$  and thickness  $h$  with various boundary conditions is analyzed under two load cases: a uniform distributed load and a central concentrated load. The geometry and material properties are shown in Fig. 2.

Due to symmetry, one quarter of plate is divided into  $N \times N$  elements. The  $12 \times 12$  meshes for the quart of the plate has been considered sufficient for engineering accuracy. The results of the KSBQP element for the central displacement  $W_C$  with various meshes are given in Table 1., and Fig. 3. Then the bending moments are listed in Table 2., for the proposed element in simply supported plate ( $W = 0$ ) and clamped plate ( $W = \beta_x = \beta_y = 0$ ) cases subjected to uniform load. The comparisons of the present results with those obtained by other authors are also plotted in Fig. 4. The results obtained using only a small number of elements prove that the new element is more efficient than other elements ACM and DKQ [5].

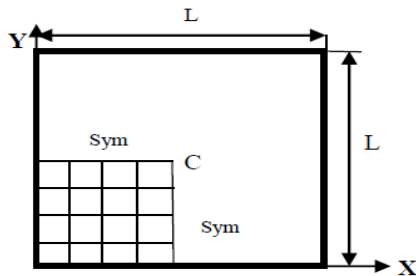


**Fig.2**  
Mesh for quadrant of square plate ( $L=20, E=10^6, \nu=0.3, P=1, q=1$ ).

**Table 1**  
Convergence of the central displacement for square plate ( $h/L=0.01$ ).

Square plate	Uniform load ( $W_c/(qL^4/100D)$ )		Central point load ( $W_c/(PL^2/100D)$ )	
	Simply supported	Clamped	Simply supported	Clamped
Mesh				
2×2	0.3992	0.1330	1.1879	0.5818
4×4	0.4022	0.1298	1.1791	0.5771
8×8	0.4052	0.1274	1.1672	0.5668
10×10	0.4054	0.1271	1.1639	0.5650
12×12	0.4061	0.1268	1.1619	0.5637
Ref solution [1]	0.4062	0.1265	1.160	0.5612

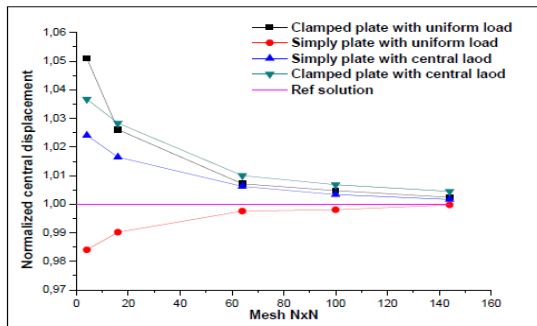


**Fig.3**  
Convergence of normalized central displacement of square plate with different boundary conditions and loadings.

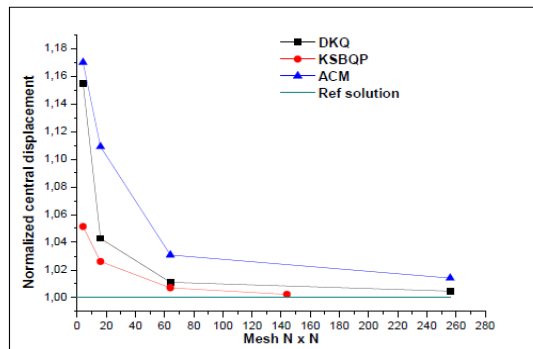


**Fig.4**  
Convergence of the normalized central displacement for clamped square plate under uniform load.

**Table 2**

Convergence of the central moment for square plate subjected to uniform load.

Mesh	Central moment	
	Clamped	Simply supported
2x2	0.0636	0.2192
4x4	0.1844	0.4284
8x8	0.2184	0.4693
10x10	0.2223	0.4705
12x12	0.2244	0.4766
Ref solution [1]	0.2291( $qL^2/10$ )	0.4789 ( $qL^2/10$ )

### 3.1.2 Twisting of square plate

A square plate simply supported ( $W=0$ ) at the corners B, C and D is shown in Fig. 5. A transverse force  $P=5$  is applied at corner A. Young's modulus is 10.000, Poisson's ratio is 0.3 and the thickness and the length of the plate are 1.0 and 8.0, respectively. The exact solution using thin plate theory is  $W_A=0.2496$  and  $W_F=0.0624$  at the center of the plate,  $M_{xy}=2.5$  and  $M_x=M_y=0$  everywhere in the plate. Results for the deflections at the points A and F, and for the moments  $M_x$ ,  $M_y$  and  $M_{xy}$  everywhere in the plate are presented in Table 3 with those of other elements. The results of KSBQP element are excellent and the two meshes provide the exact solution for the stresses and deflection.

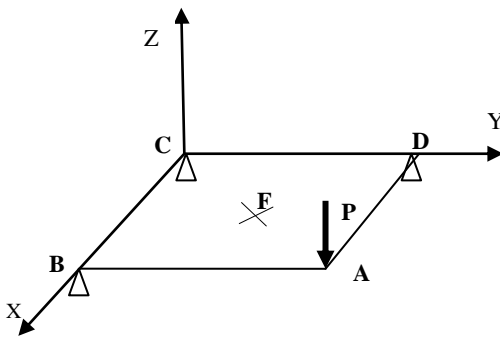


**Fig.5**  
Twisting of square plate.

**Table 3**

Deflection at points A and F for twisting square plate.

Element type	Deflection at		Moments in plate	
	Point A	Point F	Point A	Point F
KSBQP(2x2)	0.24960	0.06240	0	2.5
ACM [21](8x8)	0.24972	0.06244	-	-
HCT [21](8x8)	0.25002	0.06254	-	-
HSM [4]	0.24960	0.06240	0	2.5
DKT [4]	0.24960	0.06240	0	2.5
Exact solution [4]	0.24960	0.06240	0	2.5

### 3.1.3 Cantilever plate under a tip load

A cantilever plate shown in Fig. 6 subjected to a transverse tip load  $P=1$  at the free end is analyzed using regular and distorted meshes (Fig. 6(a) and Fig. 6(b)). This problem has been studied by Dvorkin and Bathe [22] using continuum mechanics four-node shell elements. The results of the KSBQP element given in Tables 4 and 5 indicate that the present element has good convergence for coarse mesh and the transverse displacements at free end are insensitive to the element distortions.

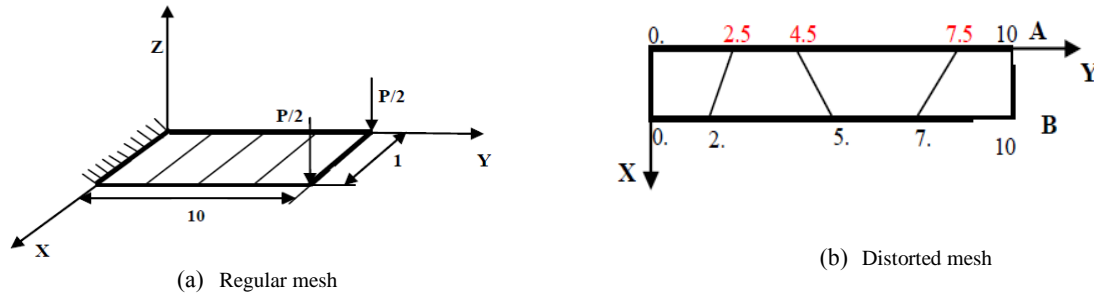


**Fig.6**  
Cantilever plate under a tip load ( $L=10, b=1, h=0.1, E=2.1 \times 10^6, \nu=0, P=1$ ).

**Table 4**  
Normalized transverse displacement of cantilever plate with regular mesh.

N	$W/W_{ref}, W_{ref} = pL^3/3EI + pL/AG$	
	KSBQP	Ref [22]
1	1.001	0.750
4	1.000	0.984

N: is the number of divisions along plate length.

**Table 5**  
Normalized transverse displacement of cantilever plate with distorted mesh.

KSBQP		Ref [22]	
$\eta_{po \text{ int } II}$	$\eta_{po \text{ int } A}$	$\eta_{po \text{ int } II}$	$\eta_{po \text{ int } A}$
1.006	1.007	0.989	0.996

$\eta = (W \text{ distorted mesh}) / (W \text{ regular mesh})$ .

### 3.1.4 Cantilever skew plate

A cantilever skew plate fixed at one side and subjected to constant pressure was analyzed using  $12 \times 12$  elements. The geometry and material properties are given in Fig. 7. In Table 6., the results for the transverse displacements at six locations are compared against the solutions obtained using other elements. It can be concluded that the proposed element gives good solution compared to experimental solution.

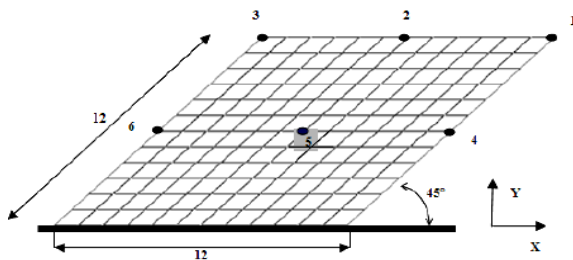


**Fig.7**  
The cantilever skew plate subjected to uniform loading ( $E = 10.5 \times 10^6, \nu = 0.35, q = 0.26066, h = 0.125$ ).

**Table 6**  
Numerical and experimental results for the cantilever skew plate under uniform load.

Elements	Mesh	Deflection at location					
		1	2	3	4	5	6
KSBQP	$12 \times 12$	0.284	0.190	0.114	0.114	0.049	0.020
HCT [21]	$8 \times 6$	0.281	0.188	0.111	0.111	0.049	0.018
DKT [4]	$4 \times 4$	0.304	0.198	0.113	0.121	0.056	0.023
4-node [22]	$4 \times 4$	0.272	0.183	0.106	0.102	0.046	0.019
16-node [22]	$2 \times 2$	0.266	0.182	0.110	0.105	0.048	0.019
Experimental [22]		0.297	0.204	0.121	0.129	0.055	0.022

### 3.1.5 Circular plate

In this study, we evaluated the performance of the present element in geometric distortion. Due to symmetry, only one quarter of a clamped or simply supported circular plate under central point  $P$  load or uniform load  $q$  was analyzed, we considered for meshing 3, 12, 48 and 192 as shown in Fig. 8. Kirchhoff's theory calculates the transverse reference displacement at the centre. The displacements obtained at the center of the circular plate are presented in Table 7., and in Figs. 9 and 10. The results of new element are in good agreement with the reference solutions [1] and accurate quickly to the reference solution.

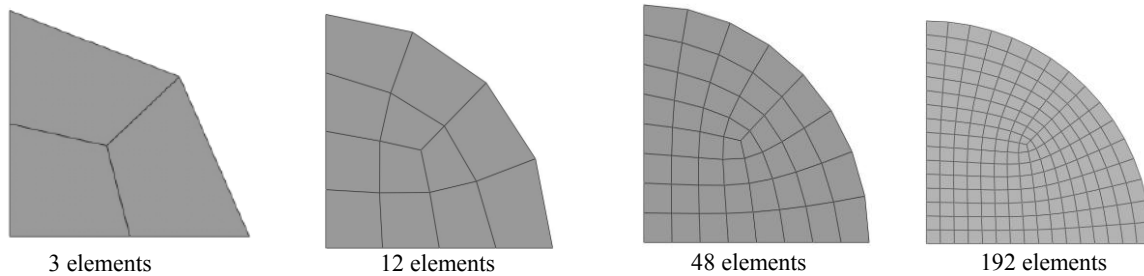


**Fig.8**  
Different meshes type of circular plate ( $R=1, E=10^{11}, \nu = 0.3, P=4000, q=1000, h=0.01$ ).

**Table 7**  
Convergence of normalized central displacements  $W_c$  for the circular plate ( $R/h = 100$ ).

NELT	Point load		Uniform Load	
	Clamped	Simply supported	Clamped	Simply supported
3	1.359	1.154	1.523	1.061
12	1.113	1.068	1.145	1.057
48	1.036	1.028	1.046	1.032
192	1.013	1.008	1.018	1.010
Ref solution [1]	$1.989PR^2/10D$	$0.5050PR^2/10D$	$0.1563 qR^4/10D$	$0.6370 qR^4/10D$

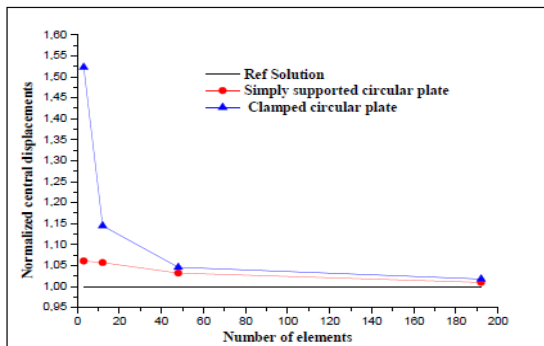


**Fig.9**  
Convergence of normalized central displacements of circular plate with uniform load.

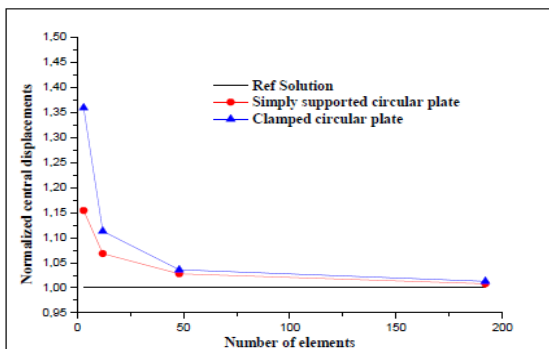


**Fig.10**  
Convergence of normalized central displacements of circular plate with Point load.

3.2 Free vibration analysis

3.2.1 Square plates

In this example, a square plate (Fig. 11) is studied to evaluate the effect of different boundary conditions on the free vibration behavior of the present element. Convergence tests of the formulated quadrilateral element is first undertaken for simply supported and clamped plates. The results of the non-dimensional frequencies ( $\bar{\omega} = \omega_{mn} a(\rho/G)^{1/2}$ ) are presented in Tables 8 and 9 and Figs. 12 and 13 with those of the ACM element. It can be observed that a faster convergence toward analytical solutions TC [23] is obtained using only a small number of elements for all cases.

Having checked the element convergence, square plates ( $h/L=0.01$ ) with various boundary conditions (SSSS, CCCC, SCSC, SCSF, SCSS and CCCF) using  $20 \times 20$  meshes are studied. The computed non-dimensional frequencies using the KSBQP element are presented in Tables 10, 11, 12, 13, 14, and 15. In Figs. 14 and 15 the error norms of frequencies for the present element and other elements have been plotted.

From numerical results, the KSBQP element shows a good performance and its results are comparable with those obtained by other plate elements (ACM element and the nine-node finite element ANSP9 [24]) and has close results to the analytical solutions TC [23] (Thin-plate closed form solution).

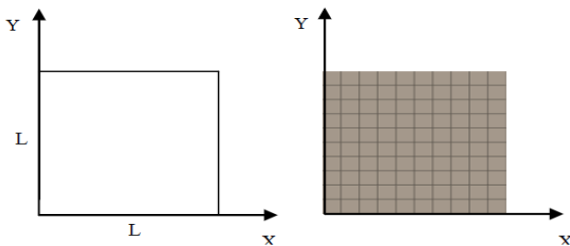


**Fig.11**  
The geometry of square plate and its FE mesh ( $E=10.92$ ,  $L=10$ ,  $\nu=0.3$ ).

**Table 8**

Convergence of natural frequencies  $\bar{\omega}$  for clamped CCCC square plate with  $h/L=0.01$ ,  $\nu = 0.3$ .

Mode	Element	Mesh divisions					TC [23]
		4 × 4	8 × 8	12 × 12	16 × 16	20 × 20	
1	KSBQP	0.1712	0.1738	0.1747	0.1751	0.1753	0.1756
	ACM	0.1674	0.1729	0.1743	0.1749	0.1751	
2	KSBQP	0.3516	0.3537	0.3559	0.3568	0.3573	0.3581
	ACM	0.3417	0.3515	0.3549	0.3562	0.3569	

**Table 9**

Convergence of natural frequencies  $\bar{\omega}$  for simply supported SSSS square plate with  $h/L=0.01$ ,  $\nu = 0.3$ .

Mode	Element	Mesh divisions					TC[23]
		4 × 4	8 × 8	12 × 12	16 × 16	20 × 20	
1	KSBQP	0.0942	0.0957	0.0960	0.0961	0.0962	0.0963
	ACM	0.0934	0.0955	0.0959	0.0961	0.0966	
2	KSBQP	0.2336	0.2385	0.2397	0.2402	0.2404	0.2408
	ACM	0.2313	0.2378	0.2394	0.2400	0.2430	

**Table 10**

Natural frequencies  $\bar{\omega}$  of a SSSS square plate with  $h/L = 0.01$ ,  $\nu = 0.3$ .

Mode	$m$	$n$	TC[23]	MC[25]	ACM	ANSP9[24]	R4	KSBQP
1	1	1	0.0963	0.0963	0.0966	0.0963	0.2079	0.0962
2	2	1	0.2408	0.2406	0.2430	0.2406	0.5917	0.2404
3	2	2	0.3853	0.3848	0.3890	0.3848	0.8358	0.3837
4	3	1	0.4816	0.4809	0.4928	0.4818	1.2930	0.4807
5	3	2	0.6261	0.6249	0.6380	0.6253	1.4454	0.6227
6	4	1	0.8187	0.8167	0.8167	0.8198	1.8958	0.8172

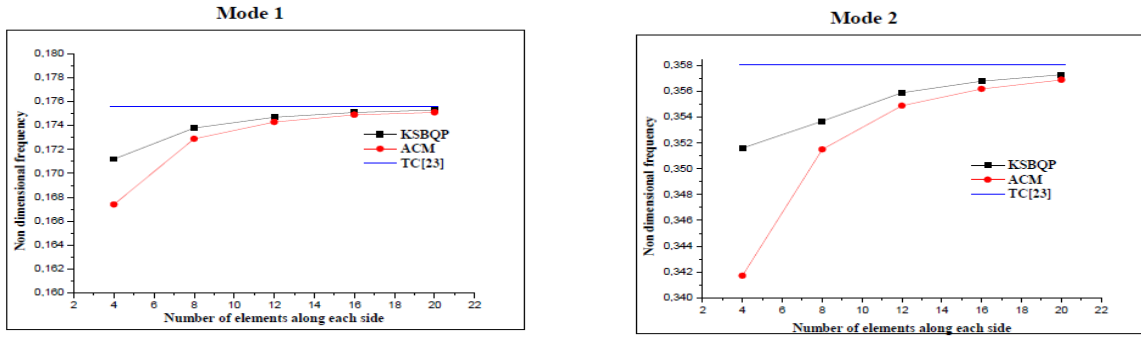


**Fig.12**  
Convergence of natural frequencies  $\bar{\omega}$  for clamped CCCC square plate.

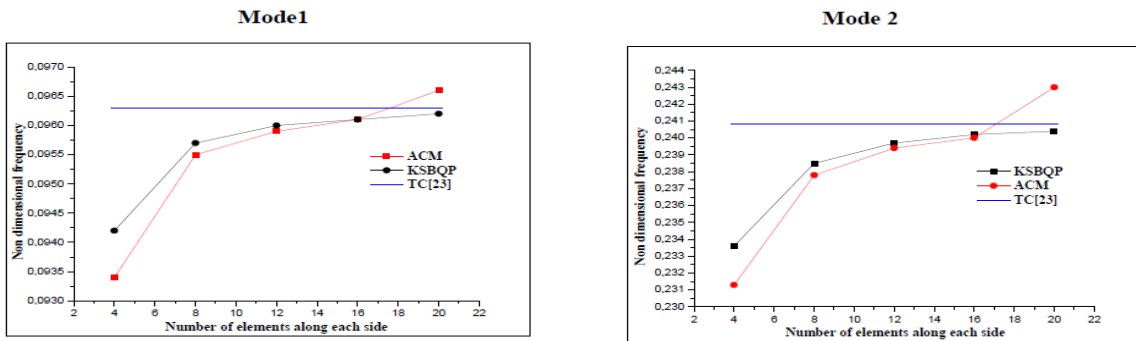


**Fig.13**  
Convergence of natural frequencies  $\bar{\omega}$  for simply supported SSSS square plate.

**Table 11**  
Natural frequencies  $\bar{\omega}$  of a CCCC square plate with  $h/L = 0.01$ ,  $\nu = 0.3$ .

Mode	$m$	$n$	TC[23]	MC[25]	ACM	ANSP9[24]	R4	KSBQP
1	1	1	0.1756	0.1754	0.1751	0.1754	0.4593	0.1753
2	2	1	0.3581	0.3576	0.3569	0.3576	0.9421	0.3573
3	2	2	0.5280	0.5274	0.5239	0.5268	1.2734	0.5251

**Table 12**  
Natural frequencies  $\bar{\omega}$  of a SCSC square plate with  $h/L = 0.01$ ,  $\nu = 0.3$ .

Mode	$m$	$n$	TC[23]	MC[25]	ACM	ANSP9[24]	R4	KSBQP
1	1	1	0.1413	0.1411	0.1409	0.1411	0.3524	0.1411
2	2	1	0.2671	0.2668	0.2661	0.2668	0.6589	0.2664
3	2	2	0.3383	0.3377	0.3375	0.3378	0.8961	0.3377
4	3	1	0.4615	0.4608	0.4584	0.4607	1.0767	0.4593
5	3	2	0.4988	0.4979	0.4970	0.4984	1.3268	0.4975
6	4	1	0.6299	0.6279	0.6284	0.6295	1.6008	0.6288

**Table 13**  
Natural frequencies  $\bar{\omega}$  of a SCSF square plate with  $h/L = 0.01$ ,  $\nu = 0.3$ .

Mode	$m$	$n$	TC[23]	MC[25]	ACM	ANSP9[24]	R4	KSBQP
1	1	1	0.0619	0.0622	0.0619	0.0619	0.1520	0.0619
2	2	1	0.1613	0.1612	0.1610	0.1612	0.3578	0.1610
3	2	2	0.2035	0.2045	0.2035	0.2034	0.5656	0.2036
4	3	1	0.3075	0.3075	0.3065	0.3071	0.6765	0.3066
5	3	2	0.3533	0.3528	0.3524	0.3528	0.9025	0.3523

**Table 14**

Natural frequencies  $\bar{\omega}$  of a SCSS square plate with  $h/L = 0.01, \nu = 0.3$ .

Mode	$m$	$n$	TC[23]	MC[25]	ACM	ANSP9[24]	R4	KSBQP
1	1	1	0.1154	0.1153	0.1152	0.1153	0.2679	0.1153
2	2	1	0.2521	0.2521	0.2514	0.2519	0.6171	0.2516
3	2	2	0.2862	0.2858	0.2855	0.2859	0.7347	0.2857
4	3	1	0.4203	0.4190	0.4177	0.4197	0.9447	0.4184

**Table 15**

Natural frequencies  $\bar{\omega}$  of a CCCF square plate with  $h/L = 0.01, \nu = 0.3$ .

Mode	$m$	$n$	TC[23]	MC[25]	ACM	ANSP9[24]	R4	KSBQP
1	1	1	0.1171	0.1171	0.1167	0.1166	0.3214	0.1168
2	2	1	0.1953	0.1951	0.1947	0.1944	0.4589	0.1947
3	2	2	0.3094	0.3093	0.3086	0.3082	0.8780	0.3087
4	3	1	0.3744	0.3740	0.3731	0.3738	0.9993	0.3732
5	3	2	0.3938	0.3931	0.3918	0.3924	0.9564	0.3923
6	4	1	0.5699	0.5695	0.5652	0.5678	1.2923	0.5661

Note: TC: Thin-plate closed form solution[23] ;MC: Reissner-Mindlin thick plate closed form[25];S – Simply supported: for the edge parallel to the  $x$ -axis ( $W=0$  and  $\beta_x=0$ ), and for the edge parallel to the  $y$ -axis ( $W=0$  and  $\beta_y=0$ ); C – Clamped:  $W=0, \beta_x=0$  and  $\beta_y=0$ .; F – Free:  $W \neq 0, \beta_x \neq 0$  and  $\beta_y \neq 0$ .

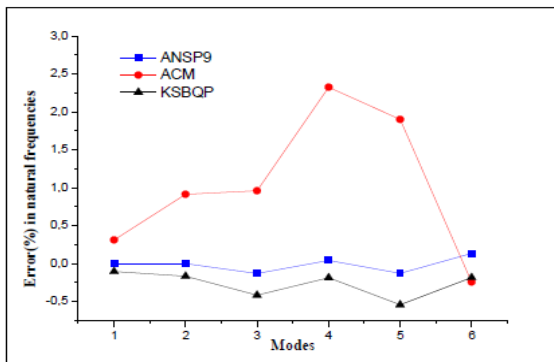


**Fig.14**  
Comparison of error norms in natural frequencies of SSSS square plate.

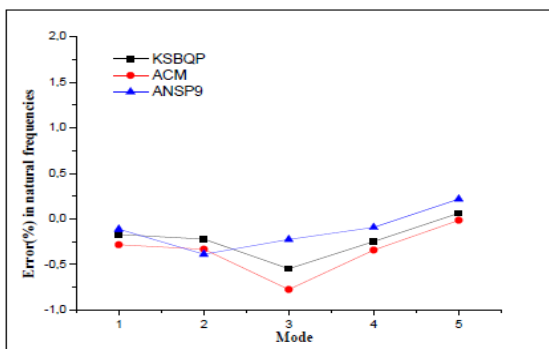


**Fig.15**  
Comparison of error norms in natural frequencies of CCCF square plate.

### 3.2.2 Transverse vibrations of simply supported thin rectangular plate

For analysis of simply supported rectangular plate, the material properties are considered as follow: Young's modulus  $E = 2 \times 10^{11} \text{ N/m}^2$ , Density  $\rho = 8000 \text{ kg/m}^3$  and Poisson's ratio is  $\nu = 0.3$ . As shown in Fig. 16, the plate has 100 mm of length and 50 mm of width. The rectangular plate is modeled with a regular mesh constituting of eight elements along the length and four elements along the width. The analytical expressions of the transverse frequencies are given by [26]:

$$f_{mn} = \frac{\pi}{2} \left( \frac{m}{L^2} + \frac{n^2}{l^2} \right) \sqrt{\frac{D}{\rho h}} \tag{30}$$

The obtained results are presented in Table 16 and Fig. 17 of a simply supported plate with  $L/h = 50$  and  $L/h = 100$ . To have a better view, Fig. 18 also shows the first four vibration modes for a simply supported plate with  $L/h = 50$ . The KSBQP element presents good results when compared to other elements and agree with the exact solution [26]. Fig. 17 shows that the KSBQP element produces more accurate results than those given by other elements (The Strain Based Brick Element SBBNN [15] and the 3D hexahedral finite element SFR8 [27]).

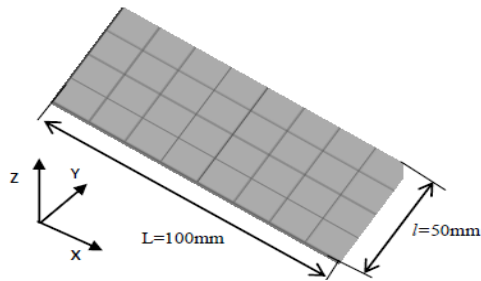


**Fig.16**  
The simply supported thin rectangular plate modeled with  $8 \times 4$  elements.

**Table 16**  
The first five transverse natural frequencies of simply supported thin rectangular plate.

	SBBNN[15]	SFR8[27]	KSBQP	Exact solution [26]
$L/h = 50$				
f11	25.062	26.447	23.564	23.767
f21	41.026	41.856	37.175	38.027
f31	70.536	69.172	60.006	61.794
f12	93.949	96.68	80.265	80.808
f22	115.94	110.34	92.228	95.068
$L/h = 100$				
f11	12.703	13.296	11.773	11.883
f21	21.211	21.136	18.587	19.013
f31	38.967	35.129	30.003	30.897
f12	50.096	49.094	40.132	40.404
f22	67.377	56.909	46.114	47.534

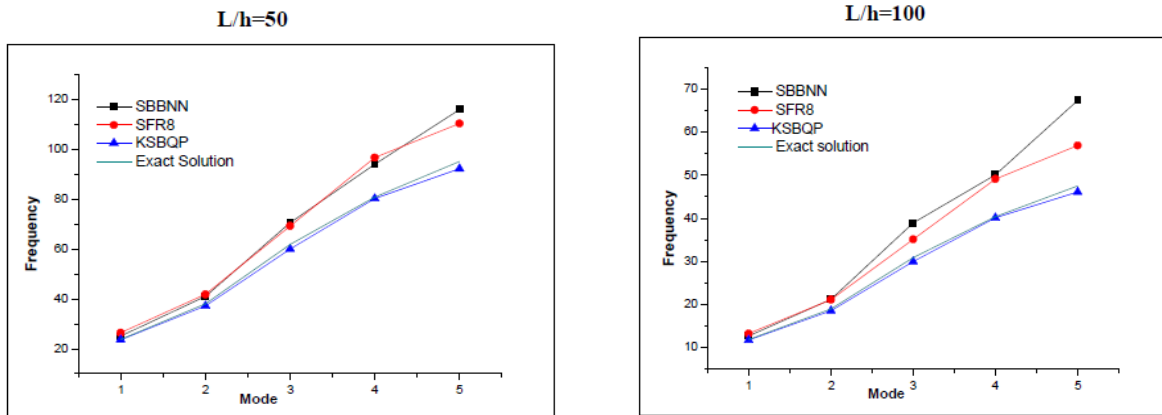


**Fig.17**  
First five transverse natural frequencies of simply supported thin rectangular plate with  $8 \times 4$  elements.

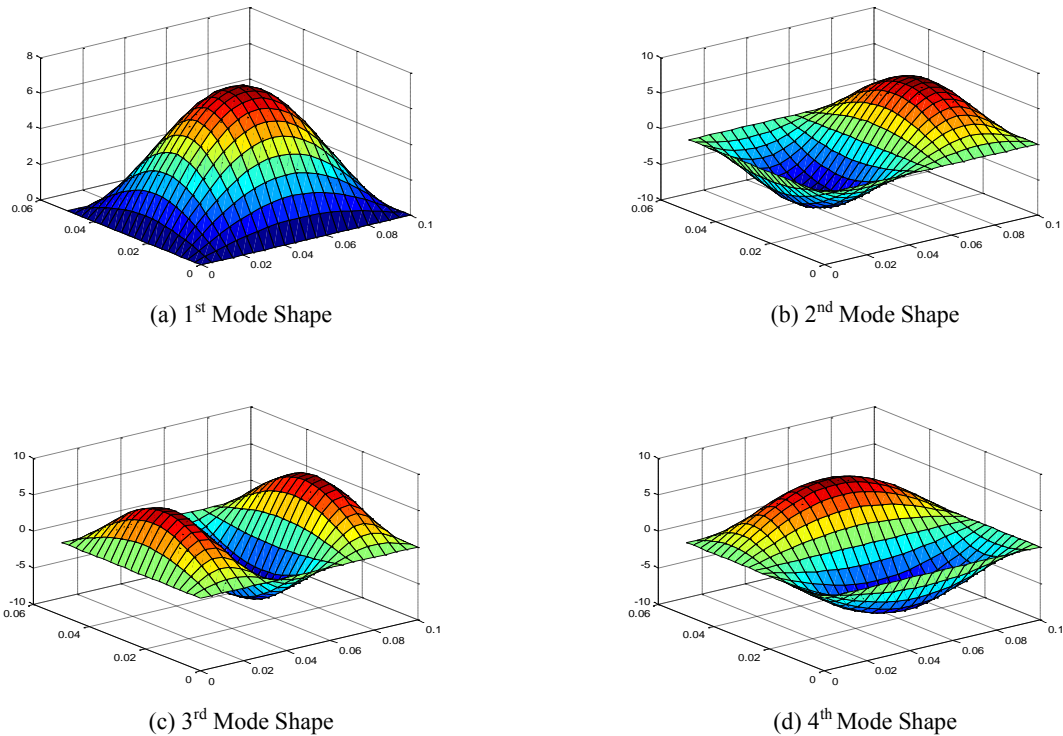


**Fig.18**  
Different mode shapes of simply supported thin rectangular plate ( $L/h=50$ ) (mesh size  $20 \times 20$ ).

3.2.3 Out-of-plane bending vibrations of a rectangular isotropic elastic beam

We consider an example of out-of-plane bending vibrations of the isotropic elastic beam which is modeled with a regular mesh constituted of 10 elements along the length and one element along the width. Geometric and mechanical data are given in Fig. 19. Analytical expressions of the transverse natural frequencies are given by [26]:

$$f_n = \frac{a_n}{2\pi} \sqrt{\frac{EI}{\rho SL^2}} ; I = \frac{bh^3}{12} ; S = b \times h \tag{31}$$

where  $EI$  is the bending stiffness of the section,  $\rho$  the mass density of the beam material and  $a_n$  a numerical constant which is different for each mode. Table 17 summarized the obtained results of only the first three numerical natural frequencies for three configurations: Clamped–Free (CF), Clamped–Clamped (CC) and Simply Supported (SS). We remark that the obtained frequencies by the present element KSBQP are more accurate than the results of the Space Fiber Rotation element SFR8 [27]. For Clamped–Free (CF) and Simply Supported (SS) configurations, SBBNN [15] element presents the most accurate results.

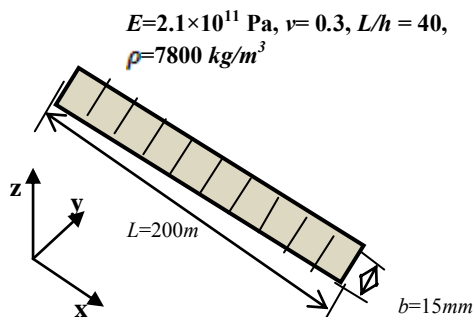


**Fig.19**  
The isotropic elastic beam modeled with  $10 \times 1$  elements.

**Table 17**  
The first three natural frequencies of the out-of-plane bending beam.

	SBBNN[15]	SFR8[27]	KSBQP	Exact solution [26]
<i>L/h = 50</i>				
f11	25.062	26.447	23.564	23.767
f21	41.026	41.856	37.175	38.027
f31	70.536	69.172	60.006	61.794
f12	93.949	96.68	80.265	80.808
f22	115.94	110.34	92.228	95.068
<i>L/h = 100</i>				
f11	12.703	13.296	11.773	11.883
f21	21.211	21.136	18.587	19.013
f31	38.967	35.129	30.003	30.897
f12	50.096	49.094	40.132	40.404
f22	67.377	56.909	46.114	47.534

3.2.4 Parallelogram plates

In this example, a parallelogram plate with a skew angle  $0^\circ \leq \theta \leq 30^\circ$  is investigated using a thickness- span ratio 0.01. The geometry of parallelogram plate is illustrated in Fig. 20. The same notation used in the previous examples is adopted to denote the boundary condition of the plate and the case S-C-S-C is used in this example. The plate is modeled with  $22 \times 22$  elements. The resulting non-dimensional frequencies ( $\bar{\omega} = \omega_{mn} L^2 / \pi^2 (\rho h / D)^{1/2}$ ) are reported in Table 18 and compared with reference solution [28] using the Ritz method (thin plate theory). The KSBQP element shows good performance and its results are in good agreement with the reference solution [28]. But there is some difference between the result of the present element and reference solution [28] in case of the plate with ( $\theta = 30^\circ$ ).

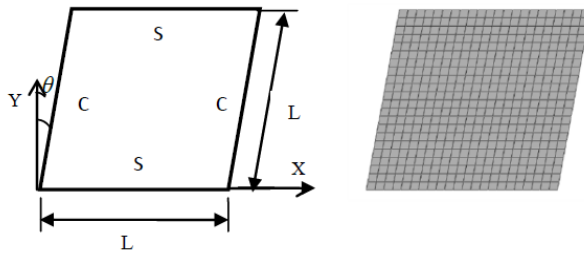


**Fig.20**  
The geometry of parallelogram plate and its FE mesh.

**Table 18**  
The parameterized natural frequencies  $\bar{\omega}$  of parallelogram plate.

$\theta^\circ$		Mode <i>n</i>							
		1	2	3	4	5	6	7	8
0	Ref sol[28]	2.933	5.548	7.024	9.586	10.361	13.080	14.210	15.690
	KSBQP	2.938	5.563	7.037	9.634	10.389	13.106	14.321	15.787
5	Ref sol[28]	2.953	5.570	7.084	9.557	10.500	13.180	14.140	15.870
	KSBQP	2.943	5.591	7.043	9.663	10.156	13.111	14.386	15.813
10	Ref sol[28]	3.014	5.641	7.266	9.529	10.860	13.500	14.030	16.340
	KSBQP	2.961	5.679	7.062	9.746	10.662	13.130	14.585	15.894
15	Ref sol[28]	3.121	5.765	7.579	9.552	11.390	13.980	14.080	16.960
	KSBQP	2.992	5.831	7.094	9.890	11.021	13.164	14.932	16.039
20	Ref sol[28]	3.276	5.955	8.040	9.699	12.100	14.050	14.910	17.750
	KSBQP	3.039	6.060	7.141	10.107	11.557	13.212	15.451	15.247
25	Ref sol[28]	3.497	6.226	8.678	9.949	13.000	14.300	16.100	18.800
	KSBQP	3.105	6.380	7.209	10.412	12.309	13.282	16.180	16.545
30	Ref sol[28]	3.797	6.598	9.539	10.300	14.100	14.700	17.800	19.600
	KSBQP	3.196	6.8209	7.300	10.833	13.335	13.378	16.960	17.183

## 4 CONCLUSION

In the current paper, a four-node quadrilateral finite element (KSBQP) was proposed for the analysis of the thin plate bending. The element possesses three usual degrees of freedom at each node. This element based on strain approach and Kirchhoff plate theory is enriched with higher-order assumed strain field. The accuracy and efficiency of the proposed plate element have been evaluated through extensive numerical tests to the static and free vibration of thin plate analyses. All results reveal that the suggested element has a good convergence in coarse meshes, highly insensitive to mesh distortion, and rapid convergence to exact solution. Finally, the present element based on the strain approach has performed well in most situations and the advantages of using the strain approach are again confirmed.

## REFERENCES

- [1] Timoshenko S., Woinowsky-Krieger S., 1959, *Theory of Plates and Shells*, London, McGraw-Hill.
- [2] Hrabok M. M., Hrudey T. M., 1984, A review and catalogue of plate bending finite elements, *Computer Structure* **19**(3): 479-495.
- [3] Melosh R. J., 1962, A stiffness matrix for the analysis of thin plates in bending, *Journal of the Aerospace Science* **29**(1): 102-103.
- [4] Batoz J-L., Bathe K-Jür., Ho L-W., 1980, A study of three-node triangular plate bending elements, *International Journal for Numerical Methods in Engineering* **15**(12): 1771-1812.
- [5] Batoz J.L., Tahar M. Ben., 1982, Evaluation of a new quadrilateral thin plate bending element, *International Journal for Numerical Methods in Engineering* **18**(11): 1655-1677.
- [6] Jirousek J., Leon N., 1977, A powerful finite element for plate bending, *Computer Methods in Applied Mechanics Engineering* **12**(1): 77-96.
- [7] Rezaiee-Pajand M., Yaghoobi M., Karkon M., 2012, Hybrid trefftz formulation for thin plate analysis, *International Journal of Computational Methods* **9**(4).
- [8] Belarbi M. T., Charif A., 1998, Nouvel élément secteur basé sur le modèle de déformation avec rotation dans le plan, *Revue Européenne des Elements Finis* **7**(4): 439-458.
- [9] Rezaiee-Pajand M., Gharaei-Moghaddam N., Ramezani, M., 2019, A new higher-order strain-based plane element, *Scientia Iranica A* **26**(4): 2258-2275.
- [10] Ashwell D. G., Sabir A. B., Roberts T. M., 1971, Further studies in the application of curved finite elements to circular arches, *International Journal of Mechanical Science* **13**(6): 507-517.
- [11] Ashwell D.G., Sabir A. B., 1972, A new cylindrical shell finite element based on simple independent strain, *International Journal of Mechanical Science* **14**: 171-183.
- [12] Belouнар L., Guenfoud M., 2005, A new rectangular finite element based on the strain approach for plate bending, *Thin-Walled Structure* **43**(1): 47-63.
- [13] Belarbi M. T., Charif A., 1999, Développement d'un nouvel élément hexaédrique simple basé sur le modèle en déformation pour l'étude des plaques minces et épaisses, *Revue Européenne des Elements Finis* **8**(2): 135-157.
- [14] Guerraiche K. H., Belouнар L., Bouzidi L., 2018, A new eight nodes brick finite element based on the strain approach, *Journal of Solid Mechanics* **10**(1): 186-199.
- [15] Messai A., Belouнар L., Merzouki T., 2018, Static and free vibration of plates with a strain based brick element, *European Journal of Computational Mechanics* **99**(1): 1-21.
- [16] Belouнар L., Guerraiche K., 2014, A new strain based brick element for plate bending, *Alexandria Engineering Journal* **53**(1): 95-105.
- [17] Khiouani H.E., Belouнар L., Houhou M. N., 2020, A new three-dimensional sector element for circular curved structures analysis, *Journal of Solid Mechanics* **12**(1): 165-174.
- [18] Belouнар A., Benmebarek S., Belouнар L., 2018, Strain based triangular finite element for plate bending analysis, *Mechanics of Advanced Materials and Structures* **1**: 1-13.
- [19] Belouнар A., Benmebarek S., Houhou M. N., Belouнар L., 2019, Static, free vibration, and buckling analysis of plates using strain-based reissner-mindlin elements, *International Journal of Advanced Structural Engineering* **11**(2): 211-230.
- [20] Belouнар A., Benmebarek S., Houhou M. N., Belouнар L., 2020, Free vibration with mindlin plate finite element based on the strain approach, *Journal of the Institution of Engineers Series C* **101**(2): 331-346.
- [21] Clough R., Tocher J., 1965, Finite element stiffness matrices for analysis of plate bending, *First Conference Matrix Methods in Structural Mechanics*.
- [22] Dvorkin E.N., Bathe K.J., 1984, A continuum mechanics based four-node shell element for general nonlinear analysis, *Engineering Computer* **1**(1): 77-88.
- [23] Leissa A.W., 1973, The free vibration of rectangular plates, *Journal of Sound and Vibration* **31**(3): 257-293.
- [24] Lee S.J., Han S.E., 2001, Free-vibration analysis of plates and shells with a nine-node assumed natural degenerated

- shell element, *Journal of Sound and Vibration* **241**(4): 605-633.
- [25] Janabi B., Hinton E., Vuksanovic D., 1989, Free vibrations of mindlin plates using the finite element method: Part 1. *Square Plates with Various Edge Conditions, Engineering Computer* **6**: 90-96.
- [26] Den Hartog J.P, 1985, *Mechanical Vibrations*, Dover Publications, New York.
- [27] Zouari W., Assarar M., Meftah K., Ayad R., 2015, Free vibration analysis of homogeneous piezoelectric structures using specific hexahedral elements with rotational DOFs, *Acta Mechanica* **226**(6): 1737-1756.
- [28] Nair P.S., Durvasula S., 1973, *Vibration of skew plates*, *Journal of Sound and Vibration* **26**(1):1-19.